

ExoMol line lists – XLVII. Rovibronic spectrum of aluminium monochloride (AlCl)

Sergei N. Yurchenko ¹, Emma Nogué,^{1,2} Ala'a A. A. Azzam^{3,4} and Jonathan Tennyson ¹★

¹Department of Physics and Astronomy, University College London, Gower Street, London WC1E 6BT, UK

²Department of Physics, Université Toulouse III – Paul Sabatier, Toulouse F-31062, France

³Department of Physics, The University of Jordan, Queen Rania Street, Amman 11942, Jordan

⁴AstroJo Institute, Amman 00962, Jordan

Accepted 2022 December 12. Received 2022 December 10; in original form 2022 November 2

ABSTRACT

A line list for two isotopologues of aluminium monochloride, Al³⁵Cl and Al³⁷Cl, is presented covering the wavelength range <0.2 µm, J up to 400, and applicable for temperatures up to 5000 K. The line lists are built using an empirical spectroscopic model consisting of potential energy curves, spin–orbit coupling curves, electronic angular momentum curves, and Born–Oppenheimer breakdown correction curves combined with ab initio dipole moments and cover the four lowest electronic states, $X^1\Sigma^+$, $A^1\Pi$, $a^3\Pi$, and $b^3\Sigma^+$. Considerable problems with the assignments of some laboratory rovibronic spectra are identified. Treatment of the states lying in the continuum is discussed. The YNAT line list is available from the ExoMol data base at www.exomol.com.

Key words: molecular data – opacity – planets and satellites: atmospheres – stars: atmospheres – ISM: molecules.

1 INTRODUCTION

The aluminium monochloride (AlCl) molecule is a well-known species in the envelope of the carbon star IRC+10216 (Cernicharo & Guelin 1987; Agundez et al. 2012). AlCl has also been detected in circumstellar envelope of the red asymptotic giant branch (AGB) stars R Dor and IK Tau (Decin et al. 2017) and recently in an S-type AGB star W Aquilae (Danilovich et al. 2021). The GChen model calculations of Woitke et al. (2018) predict that AlCl should be prominent in the atmospheres of hot exoplanets but its detection has so far been inhibited by the absence of a line list covering shorter wavelengths (Chubb et al. 2020).

There are many experimental studies of AlCl spectra (Sharma 1951; Reddy & Rao 1957; Lide 1965; Wyse & Gordy 1972; Hoeft, Topping & Tiemann 1973; Ram et al. 1979, 1982; Kumar, Khanna & Varshney 1985; Mahieu, Dubois & Bredohl 1989a,b; Hedderich, Dulick & Bernath 1993; Hensel et al. 1993; Saksena, Dixit & Singh 1998; Welz et al. 2006; Daniel et al. 2021), see also the summary by Welz et al. (2006). Recent interest in AlCl has been sparked by the proposal that it is an excellent candidate for laser cooling (Daniel et al. 2021).

An empirical AlCl line list was provided by Yousefi & Bernath (2018) and made available as part of the ExoMol data base (Wang, Tennyson & Yurchenko 2020). However, this line list only considers transitions within the $X^1\Sigma^+$ ground state ($v = 0$ to $v = 11$ and up to $J_{\max} = 200$). There have been a number of theoretical studies on the electronically excited states of AlCl, see Langhoff, Bauschlicher & Taylor (1988) and Xu, Zhang & Zhang (2020) for example, but none of them provide line lists. However, ab initio temperature-dependent

direct photodissociation cross-sections and rates for AlCl were recently reported by Qin, Bai & Liu (2021), based on multireference configuration interaction with a Davidson correction (MRCI + Q) calculations performed with an aug-cc-pV6Z basis set. Qin et al. (2021) reported MRCI potential energy curves (PECs) and transition dipole moment curves (TDMCs) for the singlet states of AlCl.

Here, we construct line lists for both the main isotopologues, ²⁷Al³⁵Cl (Al³⁵Cl) and ²⁷Al³⁷Cl (Al³⁷Cl), which cover the four lowest electronic states, $X^1\Sigma^+$, $A^1\Pi$, $a^3\Pi$, and $b^3\Sigma^+$, as part of the ExoMol project (Tennyson & Yurchenko 2012). The line lists are constructed using an empirical spectroscopic model consisting of PECs, spin–orbit curves (SOCs), electronic angular momentum curves (EAMCs), and Born–Oppenheimer breakdown (BOB) correction curves of AlCl obtained by refining ab initio curves by fitting to experimentally derived energy values of Al³⁵Cl and Al³⁷Cl. We use ab initio dipole moment curves (DMCs) and TDMCs computed as part of this work.

2 SPECTROSCOPIC MODEL

2.1 Ab initio calculations

To provide a starting point for construction of a spectroscopic model for the system having four electronic states ($X^1\Sigma^+$, $A^1\Pi$, $a^3\Pi$, and $b^3\Sigma^+$) of AlCl, we computed ab initio all relevant PECs, SOC, EAMCs, DMCs, and TDMCs at the (MRCI + Q)/aug-cc-pVQZ level of theory using program MOLPRO (Werner et al. 2012). The calculations used an (C_{2v} symmetry) active space of (11, 4, 4, 1), internally contracted state-averaging using 5, 4, 4, and 2 singlet states of symmetry 1A_1 , 1B_1 , 1B_2 , and 1A_2 , respectively, and 1, 1, and 1 triplet states of symmetry 3A_1 , 3B_1 , and 3B_2 , respectively. All

* E-mail: j.tennyson@ucl.ac.uk

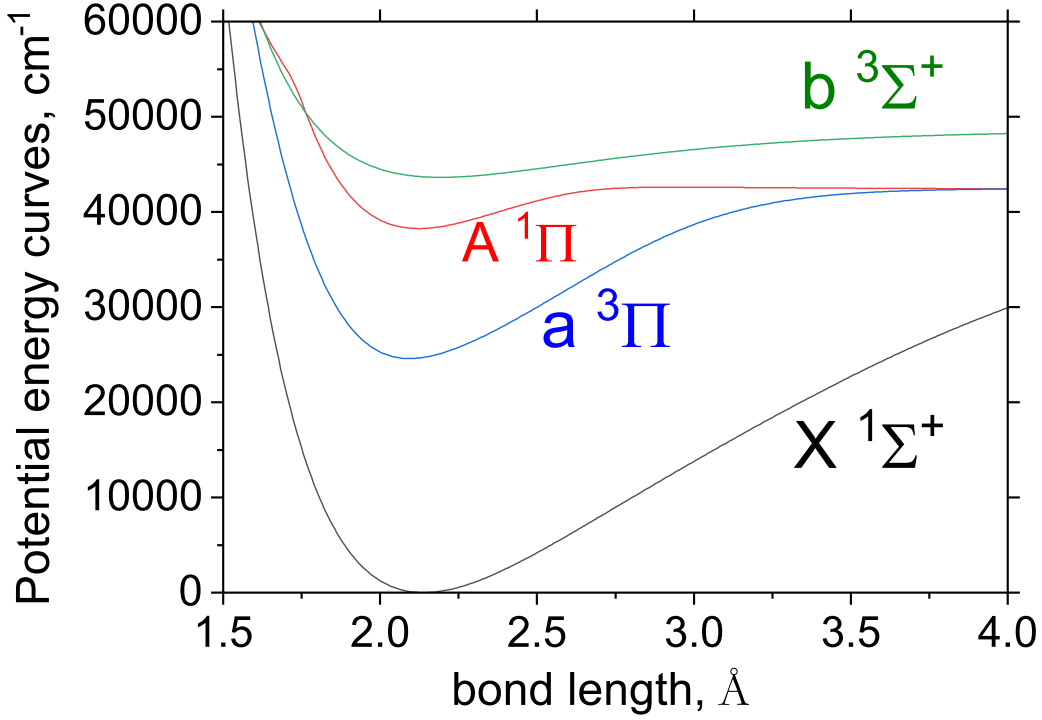


Figure 1. Refined PECs of AlCl.

curves were computed on a dense grid of non-uniformly distributed 162 points, between $r = 0.7$ and 9.5 Å.

2.2 Analytical description

To represent the PECs of the $X^1\Sigma^+$, $a^3\Pi$, and $b^3\Sigma^+$ states, the following extended Morse oscillator (EMO) function (Lee et al. 1999) was used:

$$V(r) = V_e + (A_e - V_e) \left[1 - \exp \left(- \sum_{k=0}^N B_k \xi_p^k (r - r_e) \right) \right]^2, \quad (1)$$

where A_e is a dissociation asymptote, $A_e - V_e$ is the dissociation energy, r_e is an equilibrium distance of the PEC, and ξ_p is the Šurkus variable given by

$$\xi_p = \frac{r^p - r_e^p}{r^p + r_e^p}. \quad (2)$$

The corresponding expansion parameters were obtained by fitting to the empirical [MARVEL (measured active rotation vibration energy level) and pseudo-MARVEL] energies described below.

The shallow PEC of the $A^1\Pi$ state has a small barrier to the dissociation (see Fig. 1). We used a diabatic representation for this curve constructed from two PECs $V_1(r)$ and $V_2(r)$ coupled with a diabatic term $W(r)$ as a root of a characteristic 2×2 diabatic matrix

$$\mathbf{A} = \begin{pmatrix} V_1(r) & W(r) \\ W(r) & V_2(r) \end{pmatrix}. \quad (3)$$

The lower PEC $V_1(r)$ was taken as the EMO function in equation (1). The upper PEC $V_2(r)$ is a repulsive curve playing a role of a dummy state and represented using the following hyperbolic form (in cm^{-1} and Å):

$$V_2(r) = 42\,509.8 + \frac{310\,780.97}{r^6}, \quad (4)$$

with the asymptote fixed to the asymptote of the $A^1\Pi$ state, $A_e = 42\,509.8 \text{ cm}^{-1}$. The coupling function $W(r)$ is given by

$$W(r) = \frac{1001.20}{\cosh[0.201(r - 2.668)]}, \quad (5)$$

where the parameters in equations (4) and (5) are in cm^{-1} and Å. The upper curve and the coupling curve should be considered as effective objects fitted to create the appropriate shape of the $A^1\Pi$ PEC. The two eigenvalues of the matrix \mathbf{A} are given by

$$V_{\text{low}}(r) = \frac{V_1(r) + V_2(r)}{2} - \frac{\sqrt{[V_1(r) - V_2(r)]^2 + 4W^2(r)}}{2}, \quad (6)$$

$$V_{\text{upp}}(r) = \frac{V_1(r) + V_2(r)}{2} + \frac{\sqrt{[V_1(r) - V_2(r)]^2 + 4W^2(r)}}{2}. \quad (7)$$

Only the lower component, V_{low} , is taken to represent the $A^1\Pi$ state and the other component, which is a dummy PEC, is disregarded in the rest of the calculations. In this decoupled way, we could achieve a more stable fit.

In the refinement of the SOC and the EAMC, we use the ab initio curves, which are ‘morphed’ at the ab initio grid points using the following expansion:

$$F(r) = \sum_{k=0}^N B_k z^k (1 - \xi_p) + \xi_p B_\infty, \quad (8)$$

where z is either taken as the Šurkus variable $z = \xi_p$ or a damped coordinate given by

$$z = (r - r_{\text{ref}}) e^{-\beta_2(r - r_{\text{ref}})^2 - \beta_4(r - r_{\text{ref}})^4}, \quad (9)$$

see also Prajapat et al. (2017) and Yurchenko et al. (2018). Here, r_{ref} is a reference position equal to r_e by default, and β_2 and β_4 are damping factors.

For the $X^1\Sigma^+$ state, a BOB correction curve modelled using equation (8) was used.

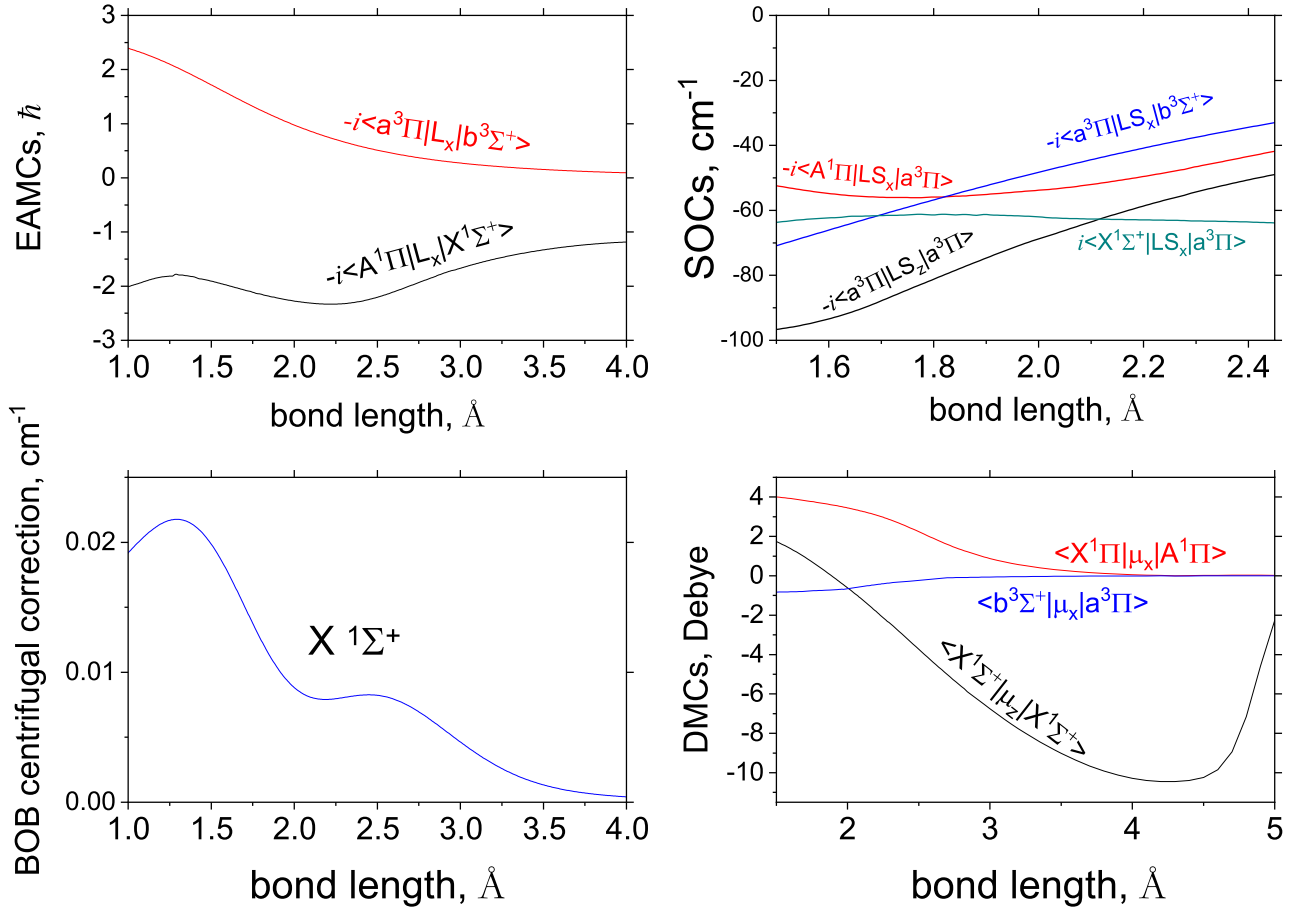


Figure 2. Refined EAMCs and SOC, a BOB curve of X , and ab initio (transition) dipole moments for AlCl.

Table 1. Summary of Al^{35}Cl experimental line positions used in the MARVEL analysis. The corresponding vibrational range is given in parentheses with each electronic state label, e.g. $X(8)$ from 72WyGo means that $v_{\text{max}} = 8$ for the state $X^1\Sigma^+$.

Reference	Tag	Range (cm^{-1})	States	N_{trans}
Lide (1965)	65Lide	0.972 526–1.458 736	$X(1)$	3
Wyse & Gordy (1972)	72WyGo	2.859 968–9.231 915	$X(8)$	69
Hensel et al. (1993)	93HeStJaMe	0.474 82	$X(0)$	1
Hoeft et al. (1973)	73HoToTi	0.972 54	$X(0)$	1
Daniel et al. (2021)	21DaWaRoHe	38 198.8042–38 240.9341	$A(1)$ – $X(1)$	31
Hedderich et al. (1993)	93HeDuBe	0.486–511.465	$A(8)$ – $X(7)$	1544
Saksena et al. (1998)	98SaDiSi	24 541.6–24 671.8	$a(0)$ – $X(0)$	270

Intensities of the ground state overtone transitions are usually sensitive to the numerical noise and tend to form non-physical plateau-like structures for higher excitations. This can be partially improved using an analytical representation of the corresponding DMC as suggested by Medvedev et al. (2015). The electronic transitions do not seem to suffer from this effect. Here, we used the double exponential decay form in equation (8) to represent the DMC of the $X^1\Sigma^+$ state. All parameters and grid values defining our spectroscopic model are provided in the supplementary material in the form of a DUO input file.

The curves representing our model are shown in Figs. 1 and 2.

2.3 MARVEL energy levels

The MARVEL procedure (Furtenbacher, Császár & Tennyson 2007; Császár & Furtenbacher 2011; Tóbiás et al. 2019) is a means of obtaining empirical energy levels by inverting high-resolution laboratory spectra. We undertook a MARVEL analysis for $^{27}\text{Al}^{35}\text{Cl}$ for which there are a number of high-resolution experimental studies available (Sharma 1951; Reddy & Rao 1957; Lide 1965; Wyse & Gordy 1972; Hoeft et al. 1973; Ram et al. 1979, 1982; Kumar et al. 1985; Mahieu et al. 1989a,b; Hedderich et al. 1993; Hensel et al. 1993; Saksena et al. 1998; Welz et al. 2006; Daniel et al. 2021). Some of these (Lide 1965; Wyse & Gordy 1972; Hoeft et al. 1973;

Table 2. Summary of Al^{35}Cl experimental line positions used in the pseudo-MARVEL analysis. The corresponding range of vibrational states is given as parentheses with each electronic state label, e.g. $A(10)$ from 82RaRuUpRa means that $v_{\text{max}} = 10$ for $A^1\Pi$.

Reference	Tag	States	Range (cm^{-1})	Transitions
Ram et al. (1982)	82RaRuUpRa	$A(10)-X(14)$, $a(0)-X(0)$, and $b(0)-a(2)$	17 754.79–38 425.9	2495
Mahieu et al. (1989a)	89MaDuBra	$A(10)-X(16)$	34 489.261–39 105.473	1938
Mahieu et al. (1989b)	89MaDuBrb	$b(0)-X(2)$	17 764.412–24 702.0173	1723

Table 3. Example of combination differences for six $A^1\Pi-X^1\Sigma^+$ transitions from 89MaDuBra (Mahieu et al. 1989a), all of which reportedly connect to the same upper state $A^1\Pi$, $v' = 8$, and $J' = 29$. The lower state energies are taken from the MARVEL set. The upper state energies are obtained using equation (10). The difference between the upper energies is significantly larger than the stated experimental uncertainty of 0.05 cm^{-1} .

v (cm^{-1})	J''	v''	E' (cm^{-1})	E'' (cm^{-1})
36 361.099	28	11	41 576.078	5214.979
35 498.610	28	13	41 575.242	6076.632
36 770.410	30	10	41 575.688	4805.278
36 334.453	30	11	41 576.055	5241.602
35 901.836	30	12	41 575.967	5674.131
35 472.368	30	13	41 575.270	6102.902

Hedderich et al. 1993; Hensel et al. 1993; Daniel et al. 2021) also consider Al^{37}Cl but the reduced amount of data available for this isotopologue was deemed insufficient to make a viable MARVEL network. Therefore, for Al^{37}Cl , we simply use the infrared emission data of Hedderich et al. (1993), which we found to be reliable for both isotopologues. This allowed us to characterize the BOB effects in the electronic ground state.

Unfortunately, not all the reports of Al^{35}Cl spectra provided data useful for MARVEL. Reddy & Rao (1957) and Welz et al. (2006) contain no assignments, while we failed to obtain a copy of Ram et al. (1979). The assignments in a number of other sources, notably Ram et al. (1982) and Mahieu et al. (1989a,b), not only proved to be inconsistent with other sources but also failed to obey combination differences within themselves. 98SaDiSi (Saksena et al. 1998) give reliable, but limited, data for the $a^3\Pi-X^1\Sigma^+$ band system. They suggest that 82RaRuUpRa (Ram et al. 1982) was misassigned and suggested an alternative assignment by shifting J values by 3. However, we found even with these new assignments, 82RaRuUpRa did not obey combination differences. Similarly, Mahieu et al. (1989a,b) cover the $A^1\Pi-X^1\Sigma^+$ band system and their exclusion left us with the only rather limited (low J) coverage of the $A^1\Pi$ state provided by Daniel et al. (2021) plus the $a^3\Pi-X^1\Sigma^+$ data of Saksena et al. (1998) to help characterize the electronically excited states. Given the need for even approximate data on the excited vibrational states of the electronic states of AlCl , use of these sources is discussed in the next section.

Table 1 presents a summary of the sources that we did include. The microwave studies due to Hoeft et al. (1973) and Hedderich et al. (1993) give hyperfine-resolved transitions; we simply averaged these transitions to provide the transitions with the same quantum numbers as the other sources. The quantum numbers used were electronic state label in PYVALEM notation (e.g. X1Sigma+), total angular momentum (J), vibrational quantum number (v), fine structure counting number (F1, F2, F3), and total parity ($p = +/−$).

The sources we retained provide 1918 transitions for Al^{35}Cl , of which 1783 form a single network yielding 1079 energy levels. Interestingly, and somewhat unusually, for these sources all tran-

sitions were validated and therefore retained in our final runs. The input MARVEL transitions file and output MARVEL energy file are provided as part of the supplementary data.

According to Mahieu et al. (1989b), the $b^3\Sigma^+$ state should actually be of $^3\Delta$ symmetry, not $^3\Sigma^+$, which they claim is consistent with the ab initio calculations of Langhoff et al. (1988), although we did not find this in Langhoff et al. or, indeed, in subsequent electronic structure publications. This assumption also does not agree with Ram et al. (1982). We could not resolve the possible two Λ components structure of a $^3\Delta$ in our analysis. Our decision to treat b as $^3\Sigma^+$ appears to provide satisfactory results.

Table 2 gives a summary of the experimental data on Al^{35}Cl not included in the MARVEL analysis due to their low resolution, large uncertainties, or inconsistent assignment. We use these data in the next paragraph via a ‘pseudo-MARVEL’ procedure based on their combination differences.

2.4 Pseudo-MARVEL energies

In the refinements, an extended set of experimental energies of Al^{35}Cl from Table 2 was constructed using ground state combination differences. The values were calculated as follows. First, the MARVEL energies described above were used as lower state energies $E_i^{(\text{low})}$ in connection with the transition frequencies ν_{ij} of Al^{35}Cl from the extended experimental set to obtain the upper state energies $E_j^{(\text{upp})}$

$$E_{j(i)}^{(\text{upp})} = E_i^{(\text{low})} + \nu_{ij}, \quad (10)$$

where the index (i) indicates the lower state i used. For the transitions to the same upper state j , this procedure allows us to obtain realistic estimates of the corresponding uncertainties of the experimental line positions. The upper state energy of the state j is then obtained by averaging $E_{j(i)}^{(\text{upp})}$ over i :

$$E_j^{(\text{upp})} = \overline{E_{j(i)}^{(\text{upp})}} \pm \Delta E, \quad (11)$$

where ΔE is the corresponding estimated uncertainty of $E_j^{(\text{upp})}$ from this averaging procedure. We call these $E_{j(i)}^{(\text{upp})}$ pseudo-MARVEL energies. We found that many transitions from the extended experimental data in Table 2 exhibit uncertainties significantly larger than those claimed in the original publications. Table 3 shows an example of combination differences for six $A^1\Pi-X^1\Sigma^+$ transitions from Mahieu et al. (1989a) connecting the same upper state. The standard deviation for the estimated upper state energies is 0.4 cm^{-1} , which is much higher than the uncertainty reported of 0.05 cm^{-1} . We set a threshold of 0.3 cm^{-1} and selected additional 910 pseudo-MARVEL energies to combine them with the pure MARVEL set of 1079 energies.

This procedure allowed us to significantly extend the vibrational coverage of the shallow $A^1\Pi$ state using the large sets of transitions provided by 89MaDuBra (Mahieu et al. 1989a) and 82RaRuUpRa (Ram et al. 1982), up to the last bound state $v = 10$. Vibrationally excited states play important role in refinements as they allow sampling larger ranges of r in the PECs. Moreover, with this

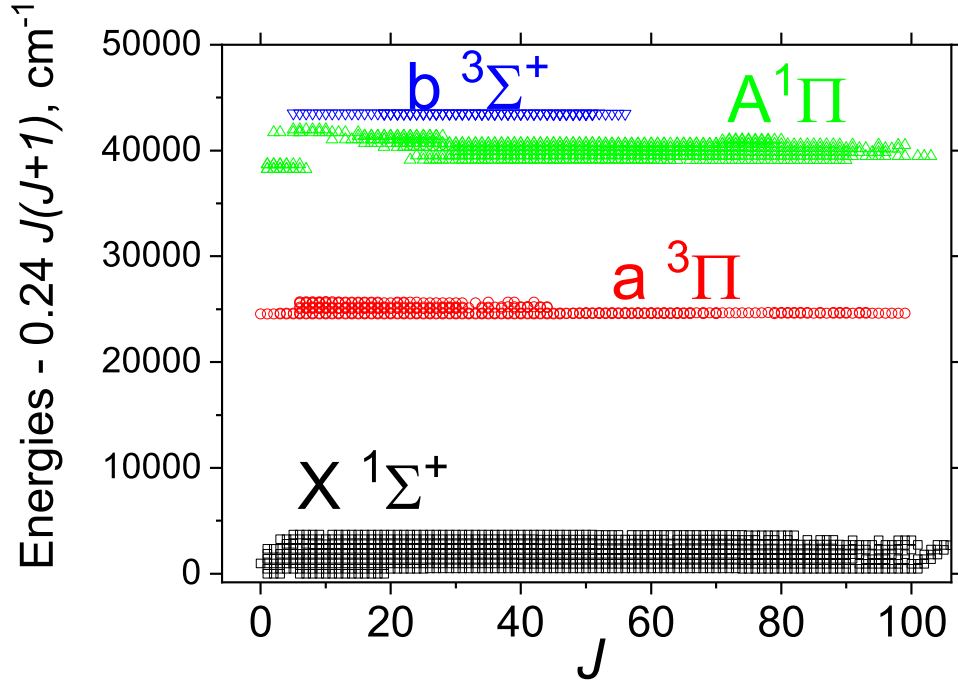


Figure 3. Illustration of the experimentally derived energy term values used of Al³⁵Cl in the refinement of the ab initio spectroscopic model.

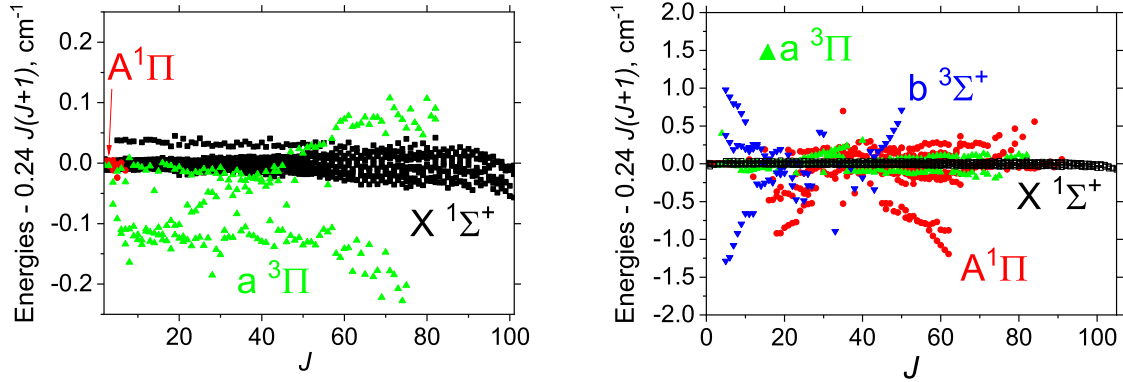


Figure 4. Al³⁵Cl obs. – calc. residuals of the refined spectroscopic model. Left-hand panel: for the MARVEL energies only; right-hand panel: all energies including pseudo-MARVEL.

Table 4. Extract from the states file of the line list for Al³⁵Cl.

<i>i</i>	Energy, \tilde{E} (cm ⁻¹)	g_i	J	unc	Parities		State	v	Λ	Σ	Ω
518	38 420.831 341	120	2	14.006000	+	e	a3Pi	28	1	-1	0
519	38 680.234 330	120	2	0.056000	+	e	A1Pi	1	1	0	1
520	38 735.883 313	120	2	14.506000	+	e	a3Pi	29	1	1	2
522	38 849.116 441	120	2	14.506000	+	e	a3Pi	29	1	-1	0
523	39 109.996 159	120	2	0.106000	+	e	A1Pi	2	1	0	1
524	39 527.266 537	120	2	0.156000	+	e	A1Pi	3	1	0	1
525	39 931.163 445	120	2	0.206000	+	e	A1Pi	4	1	0	1
526	40 320.741 268	120	2	0.256000	+	e	A1Pi	5	1	0	1

Notes. *i*: state counting number; \tilde{E} : state energy term values in cm⁻¹, MARVEL or calculated (DUO); g_i : total statistical weight, equal to $g_{ns}(2J + 1)$; J : total angular momentum; unc: uncertainty, cm⁻¹; +/–: total parity; e/f: Rotationless parity; State: electronic state; v : state vibrational quantum number; Λ : projection of the electronic angular momentum; Σ : projection of the electronic spin; Ω : projection of the total angular momentum, $\Omega = \Lambda + \Sigma$.

Table 5. Extract from the transition file of the line list for Al³⁵Cl.

f	i	A_{fi} (s ⁻¹)	$\tilde{\nu}_{fi}$
21 539	21 673	2.3075E-11	1000.000 797
9 288	9 792	4.1461E-11	1000.001 960
3 187	3 691	5.7328E-17	1000.003 651
25 069	24 923	1.1677E-14	1000.008 108
19 334	19 128	7.6969E-14	1000.009 089
5 729	5 893	3.8937E-12	1000.011 920
22 895	23 029	1.0926E-14	1000.012 113
27 105	26 959	1.3593E-12	1000.012 614
29 312	29 506	8.5757E-13	1000.014 098
4374	4 538	1.1022E-16	1000.017 250

Notes. f : upper state counting number; i : lower state counting number; A_{fi} : Einstein-A coefficient in s⁻¹; $\tilde{\nu}_{fi}$: transition wavenumber in cm⁻¹.

procedure, we were also able to reconstruct the $v = 0$ rovibronic energies of the $b^3\Sigma^+$ state up to $J = 44$ using the transitions from 89MaDuBrb (Mahieu et al. 1989b) in conjunction with the $v = 0$ energies of $a^3\Pi$. These $b^3\Sigma^+$ $v = 0$ rovibronic states also appear as upper states in the larger experimental sets 82RaRuUpRa and 89MaDuBrb that connect them to a number of $a^3\Pi$ rovibronic states, not only with $v = 0$ (covered in the MARVEL data set) but also to the fundamental and overtone states of $v = 1, 2$, important for refining the shape of the PEC of $b^3\Sigma^+$. Using the pseudo-MARVEL energies of the vibronic state $v = 0$ $b^3\Sigma^+$ as upper states, we could obtain $a^3\Pi$ $v = 1, 2$ pseudo-MARVEL energies via upper state combination differences as

$$E_{i(j)}^{(\text{low})} = \overline{E_j^{(\text{upp})}} - \nu_{ij}, \quad (12)$$

where the averaging is performed over the transitions corresponding to different upper states i connected to the same lower state j . As before, many of these combination differences suffered large uncertainties, so we applied the 0.3 cm⁻¹ threshold and derived 411 additional pseudo-MARVEL term values for the $a^3\Pi$ state. The complete MARVEL + pseudo-MARVEL set of the Al³⁵Cl energies is illustrated in Fig. 3.

2.5 Refinement

The model built from our ab initio PECs and couplings was refined using nuclear motion calculations performed with diatomic variational nuclear motion program DUO (Yurchenko et al. 2016). The rovibronic Schrödinger equation was solved for four coupled electronic states $X^1\Sigma^+$, $A^1\Pi$, $a^3\Pi$, and $b^3\Sigma^+$ using the methodology described in Yurchenko et al. (2016). The vibrational basis set was constructed by solving a set of uncoupled vibrational Schrödinger equations for each of the four electronic states using the Sinc DVR method on an equidistant grid of 500 radial points ranging from 0.7 to 4.0 Å and comprised 30, 20, 30, and 30 vibrational functions, respectively.

The $X^1\Sigma^+$ state MARVEL energies with high J have large experimental uncertainties and therefore were not strongly constrained in the fit, which is why the corresponding observed minus calculated (obs. – calc.) residuals increase at $J > 80$. All curves are given in the supplementary material as a DUO input file.

Using the experimentally derived energies of Al³⁵Cl, the PECs, SOCs, and EAMCs were refined to build an empirical spectroscopic model of Al³⁵Cl. The shallow $A^1\Pi$ state with a barrier contains bound vibrational states up to $v = 10$, all of which were included in the fit. The vibrational coverage of other states is also well represented, $v = 0-8$ for $X^1\Sigma^+$, $v = 0-2$ for $a^3\Pi$, while for the

$b^3\Sigma^+$ state, we only had $v = 0$ energies. The J excitations are up to $J = 100$ (see Fig. 3).

The (adiabatic) $b^3\Sigma^+$ curve has a double-well shape with a barrier at $r = 2.19$ Å. We could not reconstruct the full complexity of this curve and treated it using a simple one-well EMO-type PES, which effectively corresponds to the diabatic representation of this PEC. The obs. – calc. residuals of the calculated energy term values for the refined spectroscopic model are shown in Fig. 4.

For Al³⁷Cl, all the curves from the Al³⁵Cl spectroscopic model were used, where the BOB of $X^1\Sigma^+$ was refined by fitting to the MARVEL energies of Al³⁷Cl obtained from Hedderich et al. (1993). This improved the $X^1\Sigma^+$ state term values of Al³⁷Cl to the quality of the Al³⁵Cl isotopologue.

All curves representing our spectroscopic models for Al³⁵Cl and Al³⁷Cl are provided as part of the supplementary material to this paper in the form of a DUO input file.

2.6 Treating unbound states

The DUO methodology is developed for the bound-bound state problems with the effective boundary condition for the rovibronic eigenfunctions to vanish at the borders of the bond length grid. However, our electronic system above the $A^1\Pi$ state dissociation includes region where unbound solutions are possible. For example, the vibronic states of the shallow $A^1\Pi$ state are only bound for $v \leq 11$, however in our calculation, a discrete set of spurious unbound states is also produced whose eigenfunctions have the exact zero at $r = r_{\text{max}} = 4.0$ Å.

Although the DUO-bound methodology can be applied to compute unbound, continuum spectra (see Pezzella, Yurchenko & Tennyson 2021, 2022), in this work we are only interested in the bound spectrum. To the end, we identify and exclude unbound states from the line list production as follows. Unlike bound states, continuum wavefunctions $\psi_\lambda(r)$ do not vanish at large distances and are identified by the non-zero density in the small region of $\delta = 0.07$ Å at the outer border r_{max} :

$$\int_{r_{\text{max}}-\delta}^{r_{\text{max}}} |\psi_\lambda(r)|^2 dr > \epsilon, \quad (13)$$

where we use $\epsilon = 10^{-8}$.

3 LINE LIST

Using the refined spectroscopic models and the DMCs for $X^1\Sigma^+ - X^1\Sigma^+$, $X^1\Sigma^+ - A^1\Pi$, and $b^3\Sigma^+ - a^3\Pi$, we generated line lists for Al³⁵Cl and Al³⁷Cl, containing bound states only (and transitions between them). We call these the YNAT line lists.

The line lists cover $J = 0-400$ with wavenumbers from 0 to 50 000 cm⁻¹, including the $b^3\Sigma^+ - a^3\Pi$ band region. Each line list is built from two files, states and transition. They have standard ExoMol format (Tennyson, Hill & Yurchenko 2013; Tennyson et al. 2020) with the standard set of quantum numbers as generated by DUO and have been extensively described elsewhere (see e.g. Yurchenko et al. 2022). Extracts from the line list files, states and transition, are given in Tables 4 and 5.

Partition functions for Al³⁵Cl and Al³⁷Cl were generated by summing over the (MARVELized) energy levels of the YNAT line lists that extend up to $J = 400$. This should be sufficient to converge the partition sum up to $T = 5000$ K. Fig. 5 compares our results with the more approximate compilation due to Barklem & Collet (2016). As we follow the HITRAN convention (Gamache et al.

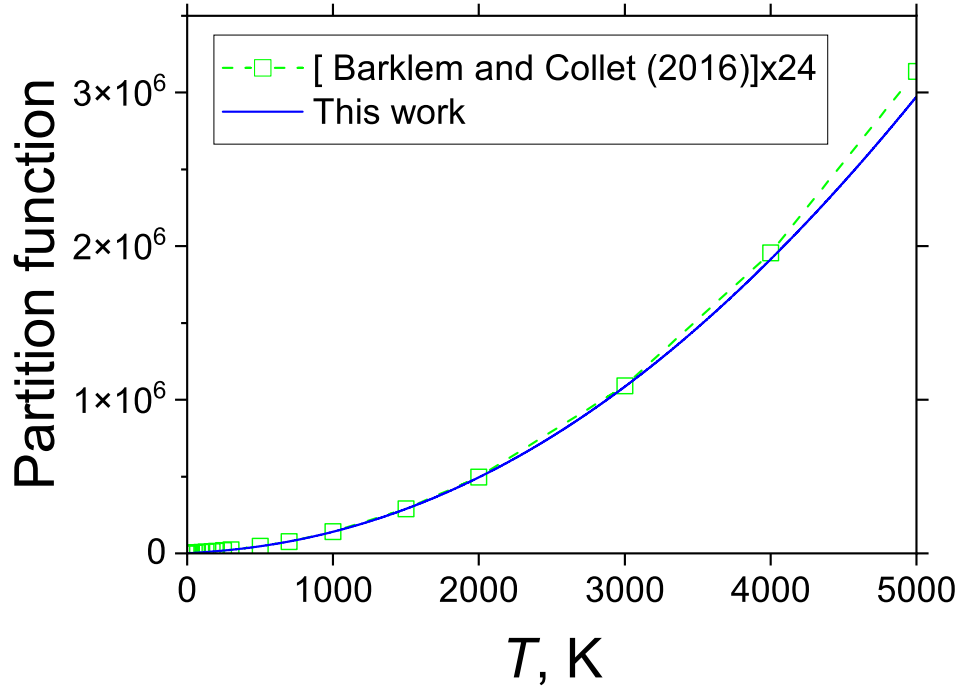


Figure 5. Partition function of Al^{35}Cl compared to that of Barklem & Collet (2016).

2017) and use the full nuclear-spin degeneracy, it is necessary to scale Barklem’s and Collet’s values. Both ^{35}Cl and ^{37}Cl have nuclear spin $I = \frac{3}{2}$ while ^{27}Al has $I = \frac{5}{2}$, which gives multiplicative factor of $(2I_{\text{Cl}} + 1) \times (2I_{\text{Al}} + 1) = 4 \times 6 = 24$ for both Al^{35}Cl and Al^{37}Cl . With this scaling, we find satisfactory agreement between the partition sums for temperatures of importance. Our partition functions for Al^{35}Cl and Al^{37}Cl are given in the supplementary data.

4 SPECTRA

Fig. 6 shows an overview of the Al^{35}Cl spectrum up to $50\,000\text{ cm}^{-1}$ for the temperature $T = 2000\text{ K}$. Besides transitions within the $X^1\Sigma^+$ ground state, the most prominent feature is the extended $A^1\Pi-X^1\Sigma^+$ band system that peaks in blue. The forbidden bands $b^3\Sigma^+-X^1\Sigma^+$ and $a^3\Pi-X^1\Sigma^+$ originate from the coupling of the corresponding states by stealing intensities from the allowed bands.

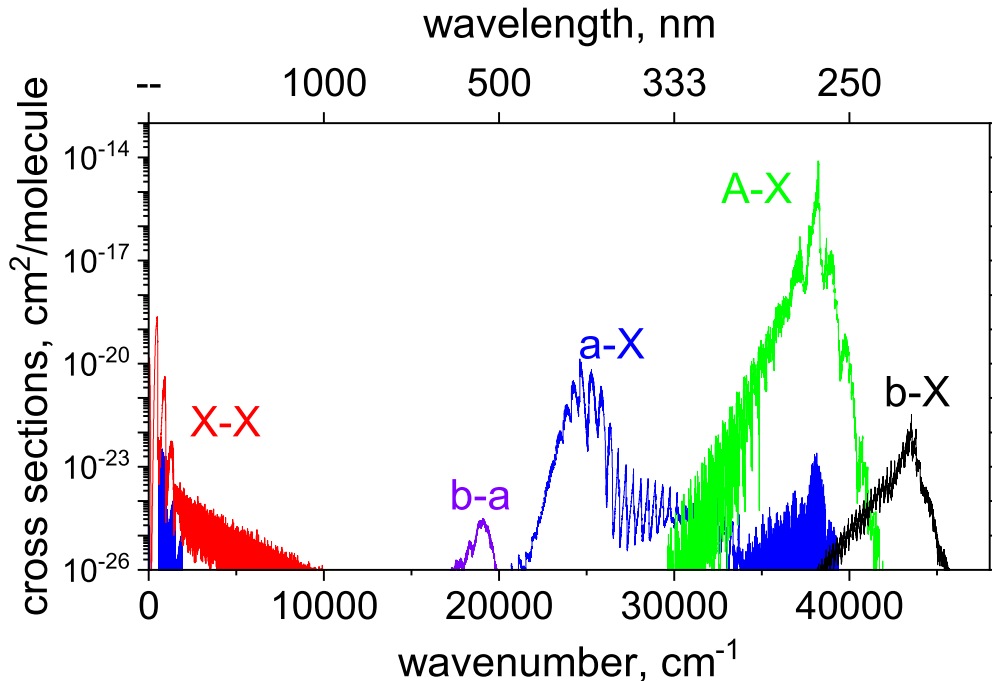


Figure 6. Overview of the YNAT absorption spectrum of Al^{35}Cl at $T = 2000\text{ K}$ using a Gaussian line profile of half-width-at-half-maximum (HWHM) = 1 cm^{-1} .

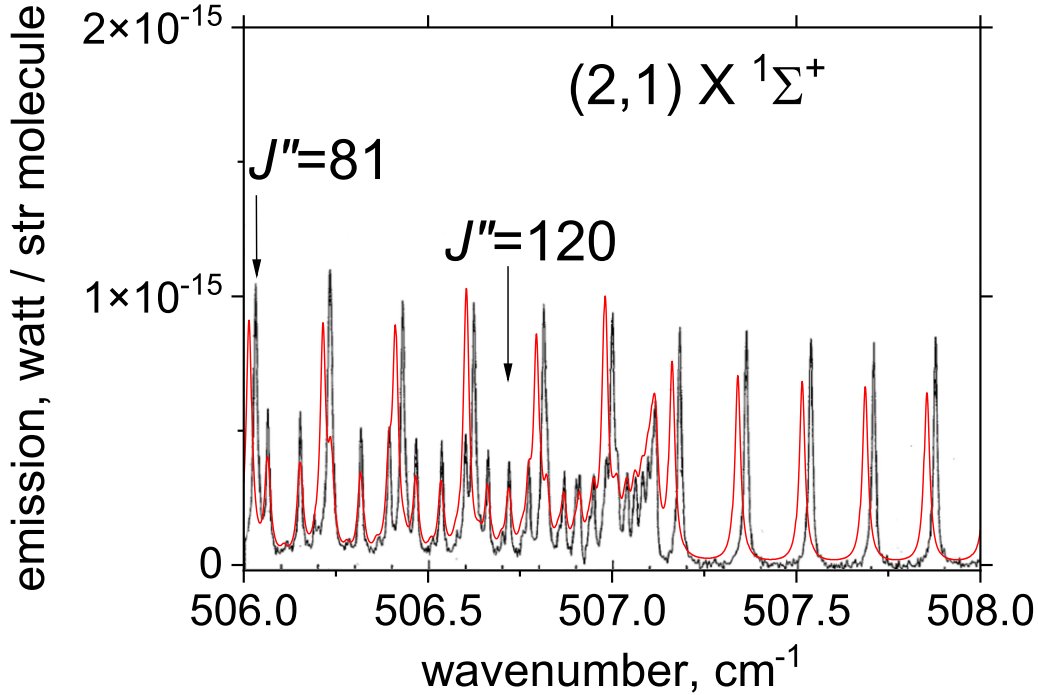


Figure 7. Comparison of the $v' = 2 - v'' = 1$ infrared band of Al^{35}Cl observed in emission by Hedderich et al. (1993) (in black) with the YNAT line list (in red) for an assumed temperature $T = 1400$ K and a Lorentzian line profile with $\text{HWHM} = 0.02$ cm^{-1} .

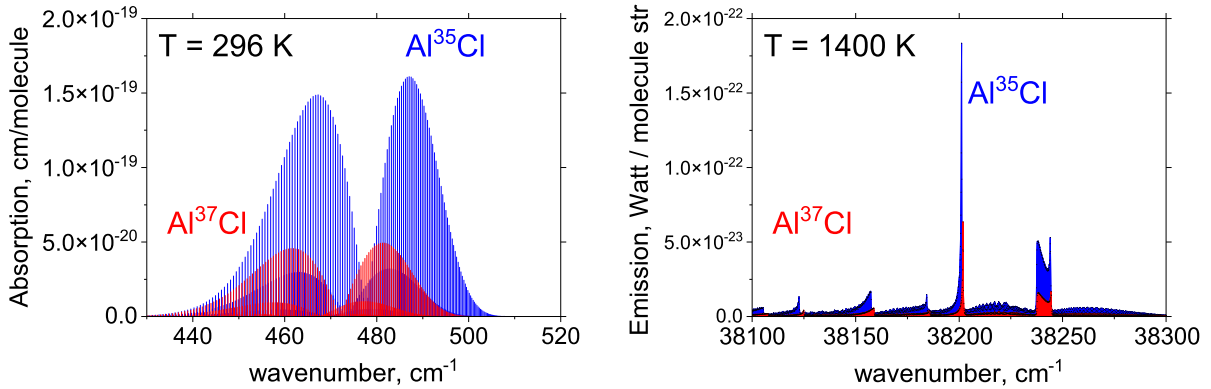


Figure 8. Two bands of two isotopologues of AlCl .

Fig. 7 compares the emission spectrum by Hedderich et al. (1993) to our simulations, showing a satisfactory agreement.

On Earth, the abundance ratio of ^{35}Cl to ^{37}Cl is close to 3:1. Fig. 8 gives two illustrative spectra of AlCl assuming a terrestrial isotope ratio.

5 CONCLUSIONS

Rovibronic line lists for two main isotopologues of AlCl are presented. These line lists, called YNAT, cover both pure bound-bound transitions and bound-quasi-bound features lying in the continuum; they are available at www.exomol.com (Tennyson et al. 2020) and www.zenodo.org (European Organization for Nuclear Research & OpenAIRE 2013). The importance of astronomical studies for correctly treating the lifetime broadening, which are a feature of quasi-bound spectra, has recently been highlighted by Yurchenko

et al. (2022). We plan to extend our treatment of such spectra to correctly allow for this in future work.

Although there have been a number of high-resolution studies of the spectrum of AlCl , we found serious problems with studies spanning many of the electronic excited states of this system. More experimental work on this problem would be welcome and would help improve the line lists.

ACKNOWLEDGEMENTS

This work was supported by the European Research Council (ERC) under the European Union's Horizon 2020 research and innovation programme through advance grant number 883830, and by STFC project numbers ST/M001334/1, ST/R000476/1, and ST/T001429/1. EN thanks Université Toulouse III – Paul Sabatier for funding her visit to UCL.

DATA AVAILABILITY

The states, transition, and partition function files for the AlCl YNAT line list can be downloaded from www.exomol.com and the zenodo. The open access program DUO is available via github.com/exomol.

REFERENCES

- Agundez M., Fonfria J. P., Cernicharo J., Kahane C., Daniel F., Guelin M., 2012, *A&A*, 543, A48
- Barklem P. S., Collet R., 2016, *A&A*, 588, A96
- Cernicharo J., Guelin M., 1987, *A&A*, 183, L10
- Chubb K. L., Min M., Kawashima Y., Helling C., Waldmann I., 2020, *A&A*, 639, A3
- Császár A. G., Furtenbacher T., 2011, *J. Mol. Spectrosc.*, 266, 99
- Daniel J. R., Wang C., Rodriguez K., Hemmerling B., Lewis T. N., Bardeen C., Teplukhin A., Kendrick B. K., 2021, *Phys. Rev. A*, 104, 012801
- Danilovich T. et al., 2021, *A&A*, 655, A80
- Decin L. et al., 2017, *A&A*, 608, A55
- European Organization for Nuclear Research, OpenAIRE, 2013, Zenodo, doi:10.25495/7GXX-RD71, <https://www.zenodo.org/>
- Furtenbacher T., Császár A. G., Tennyson J., 2007, *J. Mol. Spectrosc.*, 245, 115
- Gamache R. R. et al., 2017, *J. Quant. Spectrosc. Radiat. Transfer*, 203, 70
- Hedderich H. G., Dulick M., Bernath P. F., 1993, *J. Chem. Phys.*, 99, 8363
- Hensel K. D., Styger C., Jäger W., Merer A. J., Gerry M. C. L., 1993, *J. Chem. Phys.*, 99, 3320
- Hoefl J., Torring T., Tiemann E., 1973, *Z. Nat.forsch. A*, 28, 1066
- Kumar Y., Khanna B. N., Varshney D. C., 1985, *Indian J. Pure Appl. Phys.*, 23, 128
- Langhoff S. R., Bauschlicher C. W., Taylor P. R., 1988, *J. Chem. Phys.*, 88, 5715
- Lee E. G., Seto J. Y., Hirao T., Bernath P. F., Le Roy R. J., 1999, *J. Mol. Spectrosc.*, 194, 197
- Lide D. R., 1965, *J. Chem. Phys.*, 42, 1013
- Mahieu E., Dubois I., Bredohl H., 1989a, *J. Mol. Spectrosc.*, 134, 317
- Mahieu E., Dubois I., Bredohl H., 1989b, *J. Mol. Spectrosc.*, 138, 264
- Medvedev E. S., Meshkov V. V., Stoliarov A. V., Gordon I. E., 2015, *J. Chem. Phys.*, 143, 154301
- Pezzella M., Yurchenko S. N., Tennyson J., 2021, *Phys. Chem. Chem. Phys.*, 23, 16390
- Pezzella M., Yurchenko S. N., Tennyson J., 2022, *MNRAS*, 514, 4413
- Prajapat L., Jagoda P., Lodi L., Gorman M. N., Yurchenko S. N., Tennyson J., 2017, *MNRAS*, 472, 3648
- Qin Z., Bai T., Liu L., 2021, *MNRAS*, 508, 2848
- Ram R. S., Rai S. B., Rai D. K., Upadhy K. N., 1979, *Indian J. Phys. Proc. Indian Assoc. Cultiv. Sci. B*, 53, 56
- Ram R. S., Rai S. B., Upadhy K. N., Rai D. K., 1982, *Phys. Scr.*, 26, 383
- Reddy S. P., Rao P. T., 1957, *Can. J. Phys.*, 35, 912
- Saksena M. D., Dixit V. S., Singh M., 1998, *J. Mol. Spectrosc.*, 187, 1
- Sharma D., 1951, *ApJ*, 113, 210
- Tennyson J., Yurchenko S. N., 2012, *MNRAS*, 425, 21
- Tennyson J., Hill C., Yurchenko S. N., 2013, in Gillaspay J. D., Wiese W. L., Podpaly Y. A., eds, *AIP Conf. Proc. Vol. 1545, Atomic and Molecular Data and their Applications: ICAMDATA-2012*. Am. Inst. Phys., New York, p. 186
- Tennyson J. et al., 2020, *J. Quant. Spectrosc. Radiat. Transfer*, 255, 107228
- Tóbiás R., Furtenbacher T., Tennyson J., Császár A. G., 2019, *Phys. Chem. Chem. Phys.*, 21, 3473
- Wang Y., Tennyson J., Yurchenko S. N., 2020, *Atoms*, 8, 7
- Welz B., Becker-Ross H., Florek S., Heitmann U., 2006, *Electron Excitation Spectra of Diatomic Molecules*. Wiley, New York, p.158
- Werner H.-J., Knowles P. J., Knizia G., Manby F. R., Schütz M., 2012, *WIREs Comput. Mol. Sci.*, 2, 242
- Woitke P., Helling C., Hunter G. H., Millard J. D., Turner G. E., Worters M., Blecic J., Stock J. W., 2018, *A&A*, 614, A1
- Wyse F. C., Gordy W., 1972, *J. Chem. Phys.*, 56, 2130
- Xu J.-G., Zhang C.-Y., Zhang Y.-G., 2020, *Chin. Phys. B*, 29, 033102
- Yousefi M., Bernath P. F., 2018, *ApJS*, 237, 8
- Yurchenko S. N., Lodi L., Tennyson J., Stoliarov A. V., 2016, *Comput. Phys. Commun.*, 202, 262
- Yurchenko S. N., Sinden F., Lodi L., Hill C., Gorman M. N., Tennyson J., 2018, *MNRAS*, 473, 5324
- Yurchenko S. N. et al., 2022, *MNRAS*, 510, 903

SUPPORTING INFORMATION

Supplementary data are available at *MNRAS* online.

Data comprise the Al³⁵Cl MARVEL (input) transitions and MARVEL (output) energy levels plus a sample DUO input file that specifies potentials, couplings, and dipoles as well as the basis sets used for the nuclear motion calculations.

Please note: Oxford University Press is not responsible for the content or functionality of any supporting materials supplied by the authors. Any queries (other than missing material) should be directed to the corresponding author for the article.

This paper has been typeset from a \LaTeX file prepared by the author.